Comparison of Anatase Titania to Titanate Nanotubes in a Thin-Film Dye-Sensitized Solar Cell with Liquid and Solid Electrolyte

Daniel T. Brosnan

A thesis submitted to the faculty of the University of North Carolina at Chapel Hill in partial fulfillment of the requirements for the degree of Master of Science in the department of Physics and Astronomy

Chapel Hill
2011

Approved by:

Advisor: Professor Laurie McNeil

Reader: Professor Yue Wu

Reader: Professor Rene Lopez

Abstract

DANIEL BROSNAN: Comparison of Anatase Titania to Titanate Nanotubes in a Thin-Film Dye-Sensitized Solar Cell with Liquid and Solid Electrolyte
(Under the direction of Professor Laurie McNeil)

In this project, the properties of anatase titanium dioxide and titanate nanotubes were compared with respect to their function as a constituent material for the active layer of a dye-sensitized solar cell. A common cell configuration was used to examine the variation of cell function as a result of differences in composition, use of a solid or liquid electrolyte, and variation of processing and chemical treatment procedure, as well as the interaction of these varied parameters.

The work performed in this study consisted of the development of a cell configuration demonstrating good photovoltaic characteristics and repeatable manufacture, determination of parameters relevant to the performance of these photovoltaic devices, manufacture of a set of devices to examine the effects of variation of these parameters, and testing of these devices under standardized conditions to enable comparison of the devices to each other and to published results, as well as to elucidate the underlying causes of observed performance differences.

A performance difference between the anatase and nanotube electrodes is demonstrated, with the anatase devices performing as well as or better than nanotube devices for all preparatory conditions, and experiencing a further gain in performance from the substitution of a plasticized polymer electrolyte for the standard liquid electrolyte, compared to no change or worsened performance for nanotube based devices.

Acknowledgements

This material is based upon work supported as part of the UNC EFRC: Solar Fuels and Next Generation Photovoltaics, an Energy Frontier Research Center funded by the U.S. Department of Energy, Office of Science, Office of Basic Energy Sciences under Award Number DE-SC0001011.

I am grateful to UNC CISMM for access to the scanning electron microscope used for materials analysis in this study, and to UNC CHANL for access to the clean room facilities used in some stages of materials preparation.

The members of my committee, Professor Laurie McNeil, Professor Rene Lopez, and Professor Yue Wu, have been indispensably helpful with both ideas and access to equipment and facilities.

Thanks are also due to Dr. Bengt-Erik Mellander of Chalmers University of Technology, who provided useful insights about polymer electrolyte materials and the specific recipe used in this investigation.

I would additionally like to thank fellow graduate students Rudresh Ghosh, Courtney Hadsell, and Zheng Ren for enlightening discussions about materials and technical concerns.

Table of Contents

I: Introduction

Dye-sensitized solar cells use relatively simple manufacturing procedures and inexpensive materials to produce photovoltaic devices of relatively high efficiency. A typical device consists of a sensitized metal oxide anode immersed in an electrolyte which replenishes the electrons lost to photocurrent, which is itself replenished at a counterelectrode. Despite the promise of this configuration, such devices suffer from scientific and engineering issues which limit their utility. The most efficient examples of the technology contain a liquid electrolyte layer, using solutions of iodine and iodide salts in acetonitrile.[1] This volatile solution tends to evaporate through even a small breach in the cell containment, requiring a bulky double-layer sealed configuration[1] which effectively doubles the weight of the cell compared to a single layer.

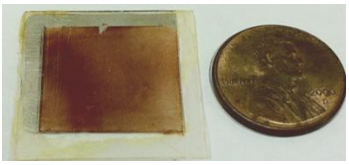

Figure 1: DSSC, viewed from active side. Platinum electrode visible to upper left.

There has been a tremendous number of variations on the original device made and tested since the publication of the original 1991 paper by O'Regan and Grätzel[2], focusing on every aspect of the device. Many electrodes, dyes, electrolytes, and counterelectrodes have been examined for their ability to reduce cost, eliminate the need for a liquid layer, or improve the photocurrent generation characteristics of the device.

A basic, unmodified dye-sensitized solar cell consists of anatase titanium dioxide spread as a paste on a glass electrode coated in a transparent conducting oxide and heat treated. This is then immersed in a solution of dye, generally a ruthenium-centered

molecule with attached bipyridyl groups, with those in turn attached to carboxyl groups to anchor them to the titania. The active area of the cell is typically surrounded by a polymeric spacer a few microns thick which serves as the wall of a cavity when the back electrode (typically platinum-coated glass) is applied. This cavity is then filled with a solution of iodine and iodide salt (often lithium iodide) in acetonitrile and the device is sealed. Efficiency for well-made devices of this type, with optimal components and processing, can approach 10%[1], which compares reasonably well to 24% for single-crystal silicon, 13% for amorphous silicon photovoltaics, and 1-3% for organic cells[3].

Physics of the Dye-Sensitized Solar Cell

Dye-sensitized cells are similar in function to other excitonic solar cells, but differ in a few key ways. Generally speaking, excitonic solar cells rely on absorbed photons to elevate a carrier to the conduction band of the device material, producing an exciton which is then dissociated at an interface. The electron is conducted to the cell anode through an n-type semiconductor, while the hole is either conducted to a cathode through a p-type medium or is chemically reduced.[3]

This scheme introduces a number of challenges, principally the fact that exciton lifetime before recombination is typically measured in nanoseconds, giving them a diffusion length of a few nanometers before recombination[4]. This makes it necessary to ensure that exciton creation occurs near an interface (preferably within the exciton diffusion length). Bulk heterojunction cells address this by blending immiscible semiconductors to distribute the boundary throughout the cell, while dye-sensitized cells localize the excitation to individual “antenna” molecules.[5]

Without sensitization, the optical absorption of nanocrystalline anatase TiO_2 is limited by its 3.2eV bandgap[6]. Photoelectrons are produced from light absorption, but with an absorption edge in the ultraviolet range, only about four percent of the total power provided by solar irradiance can be absorbed by an unsensitized anatase photocell.[6] This is remediated by the addition of a monolayer of dye molecules, exploiting the high surface area of the nanocrystalline electrode.

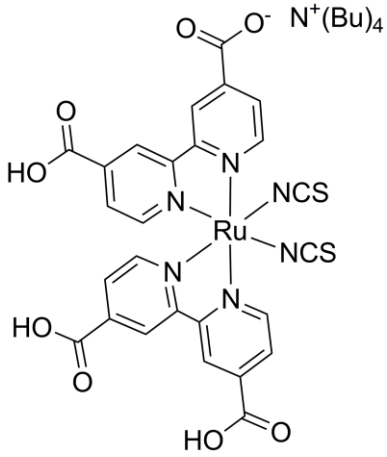

Figure 2: N719 molecule .Thiocyanated Ruthenium bipyridyl, with tetrabutylammonium ion and carboxylic acid adsorption functionality.

The most widely-used dyes are ruthenium bipyridyl molecules, carrying carboxylate or carboxylic

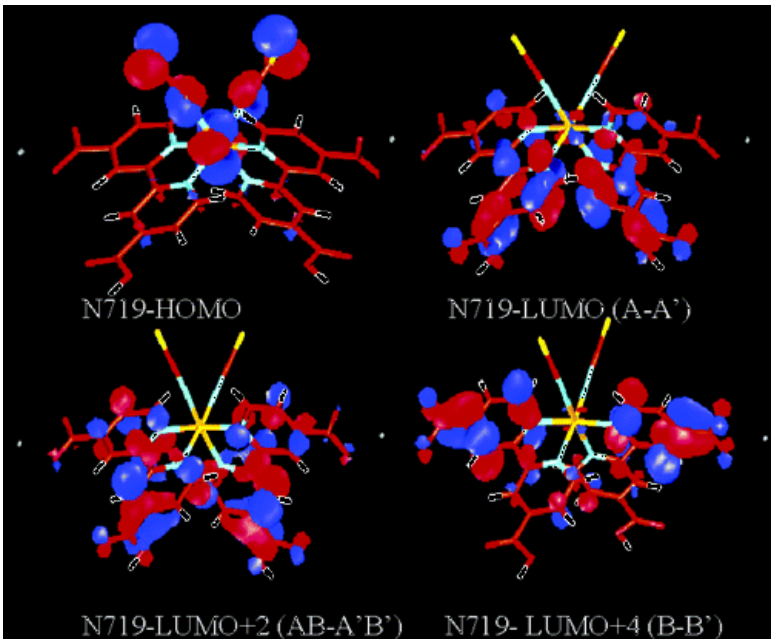

Figure 3: The DFT calculated spatial distribution of HOMO and LUMO for N719, showing localization. Image adapted from reference 5.

acid functionalities for bonding to the titania. Specifically, the devices manufactured here are sensitized with bis(tetrabutylammonium)-[*cis*-di(thiocyanato)-bis(2,2'-bipyridyl-4-carboxylate-4'carboxylic acid)-ruthenium(II)] (figure 2), typically referred to as N719. The addition of these adsorbed dye molecules extends the photon absorption of the titania into the visible range. The spatial configuration (figure 3) and energetics of the molecular HOMO and LUMO of N719 also serve to promote charge transfer and reduce the rate of recombination[7]. The N719 HOMO has an energy below that of the TiO_2 conduction band, and is localized to the ruthenium center and thiocyanate functionalities. These groups are uninvolved in surface attachment, and spatially distant from the carboxylate and carboxylic acid functionalities which connect the molecule to the titania. The LUMO spatial distributions are concentrated on the bipyridyl parts of the molecule, in much closer proximity to the bonding functionalities, and with energy above that of the TiO_2 conduction band (figure 4).

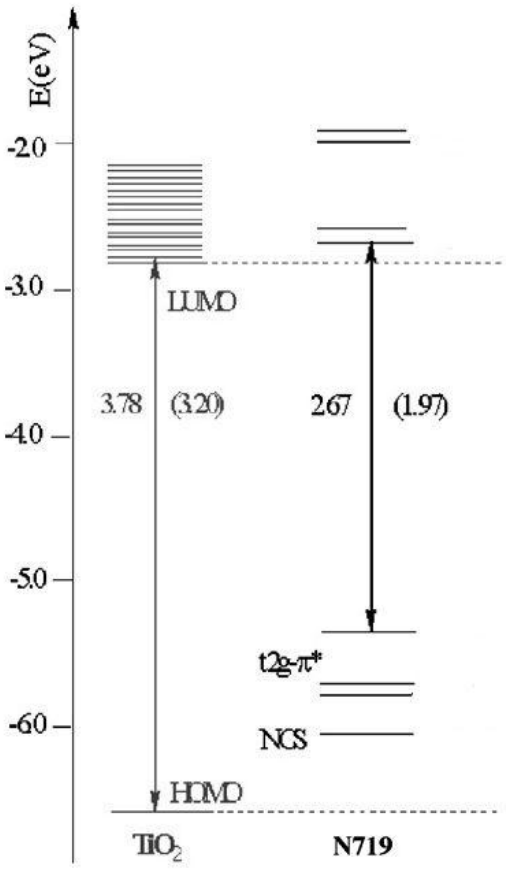

Figure 4: HOMO and LUMO energies of N719 relative to valence and conduction band of TiO_2. Adapted from ref. 8.

With the addition of a dye, the photoinduced excitation is localized to a molecular excited state, and the interface at which

charge separation occurs is the bond attaching the dye to the titania. For this system, most published works exchange a description in terms of excitons, electrons, and holes for descriptions of molecular oxidation and reduction. Photon absorption results in a molecular excited state from which an electron is transferred to the titania, raising the oxidation state of the dye's ruthenium center from Ru(II) to Ru(III)[5]. The electron travels through the titania by diffusion, as the potential difference across the cell is locally screened by the bicontinuous and interpenetrating networks of the anodic titania and the redox medium.[9]

Remediation of the dye's oxidation state is accomplished by a shuttling, ionic redox medium with two available oxidation states. Generally speaking, the electrolyte is composed of a solution of iodine and iodide salt, resulting in a slow redox cycle:

At TiO_2: $3I^- + 2dye^* \Rightarrow I_3^- + 2e^- + 2dye* \Rightarrow I_3^- + 2dye$

At Pt: $I_3^- + 2e_{Pt}^- \Rightarrow 3I^-$

In this process, transport between the titania anode and the platinum cathode occurs by ionic diffusion.[10]

Losses and inefficiency in the dye-sensitized solar cell stem from a number of sources. Incomplete absorption is the simplest such cause; reflection from the cell surface and the gaps in the dye's absorption spectrum result in the loss of some of the irradiance over the device area[5]. Absorption by the solute iodine results in further losses and the production of iodine radicals[5,11]. Once absorption by the dye and charge transfer to the titania have occurred, the primary loss processes are those of parasitic recombination by reduction of triiodide at the titania surface[11], and resistive losses as the electrons transfer

through the titania network. This is often remediated by a treatment of the titania with 4-*tert*-butylpyridine, which forms an organic layer, infiltrating pores too small to be accessed by the dye and adsorbing to sites between dye molecules, limiting contact between the redox medium and unsensitized titania and blocking recombination.[5,12]

The electrical parameters of solar cells are typically described in terms of an equivalent circuit model. A nearly-ideal solar cell has a current-voltage characteristic which can be described in terms of a current source, a diode, and series and parallel resistors (figure 5). Since this model is

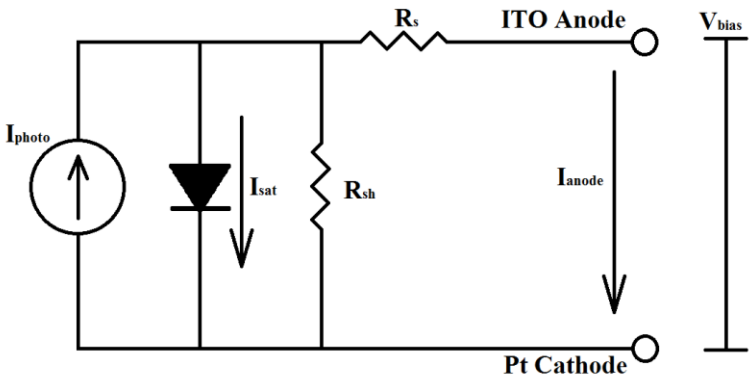

Figure 5: Equivalent circuit diagram for a photovoltaic device with applied bias.

applied to an external I/V measurement on the device, the quantities which can be directly measured are the current through the anode (I_{anode}) and the bias applied across the cell (V_{bias}), with dependence on the actual current generated by photon absorption (I_{photo}), and saturation current due to the diode nature of the device (I_{sat}) with ideality factor *m*, as well as representation of parasitic back-reaction as a shunt resistance (R_{sh}) and throughput resistance as a series resistance (R_s). This leads to an equation which describes the anode current[13]:

$$I_{anode} = I_{photo} - I_{sat} e^{\frac{-q(V_{bias}+I_{anode}*R_s)}{mkT}} + \frac{V_{bias} + I_{anode} * R_s}{R_{sh}}$$

In the case of an ideal or nearly ideal device, the series resistance is negligible, the shunt resistance is approximately infinite, and the device quality factor, *m*, is near unity. The expression then simplifies to:

$$I_{anode} = I_{photo} - I_{sat} e^{\frac{-qV_{bias}}{kT}}$$

References:

1. M. Grätzel, *J. Photochem. Photobiol. C*, **4**, 145 (2003)
2. M. Grätzel, B. O'Regan, *Nature*, **353**, 737 (1991)
3. M. Grätzel, *Nature*, **414**, 338 (2001)
4. D. Gebeyehu et al., *Synth. Met.*, **125,** 279 (2002)
5. M.K. Nazeeruddin et al, *J. Am. Chem. Soc.* **115**, 6382 (1993)
6. Y-H. Tseng et al, *Nanotechnology* **17**, 2490 (2006)
7. M.K. Nazeeruddin et al, *J. Am. Chem. Soc.*, **127**, 16835 (2005)
8. M.K. Nazeeruddin et al, *J. Photochem. Photobiol. A.*, **185**, 331 (2007)
9. A. Zaban, A. Meier, B.A. Gregg, *J. Phys. Chem. B.*, **101**, 7985 (1997)
10. A. Hauch, A. Georg, *Electrochim. Acta*, **46**, 3457 (2001)
11. J. Rowley, G.J. Meyer, *J. Phys. Chem. C. Lett.*, **113**, 18444 (2009)
12. H. Lindström et al, *J. Phys. Chem.*, **100**, 3084 (1996)
13. J. Halme, P. Vahermaa, K. Miettunen, P. Lund, *Adv. Mater.*, **22** E210 (2010)

II: Experimental

Preparation of Materials

Titanate Nanotubes

Titanate nanotubes as used in this study were made in a wet chemical process wherein they were heated in an aqueous alkaline environment. The alkaline solution consisted of 24g sodium hydroxide, added to 60mL deionized water and stirred until dissolved. To this, 600mg titanium dioxide (Degussa, P25) was added. This solution was placed in a Teflon reaction vessel which was enclosed in a steel autoclave jacket and heated in an oven at 140C for 72 hours.

After cooling to room temperature, the solution was removed from the pressure vessel and the solid material was pulverized. The suspension was then sonicated for 45 minutes. At this point, suspended nanotubes were collected by centrifugation, the supernatant was removed, and 0.1M HCl in distilled water was added. This was then agitated and centrifuged, and the HCl wash, agitation, and centrifugation process was repeated until the removed supernatant is of neutral pH. This process produced hydrogenated titanate material ($H_2Ti_3O_7$) with nanotubular (or nanoscrolled) morphology.[14]

In suspension, there is an observable variation of aggregate size, with some aggregates of millimeter size quickly settling out, micron-sized aggregates settling out over

a period of hours to days, and nanometer aggregates and free tubes tending to remain suspended. The largest aggregates can be reduced by bulk grinding with a mortar and pestle, and extended sonication tends to produce more suspension-stable and smaller particles as well. If the material is collected from solution and allowed to dry, it will form new aggregates as the solvent evaporates.

Electrolyte Solutions

The electrolytes used in this study are based on the typical I_2^-/I_3^- redox system used in most DSSC devices[15], with a 10:1 mass ratio of iodide salt to iodine in a solid or liquid medium.

The solid electrolyte is made by dissolving a 1:1 ratio poly(ethylene oxide) (4,000,000 g/mol, Sigma Aldrich) and ethylene carbonate in anhydrous acetonitrile (60mL per gram PEO), followed by the addition of tetra-*n*-hexylammonium iodide and iodine at a mass ratio of 10:I_2, and 0.15g THAI per gram PEO[16].

The liquid electrolyte is made with the same amount of iodine and iodine salt mass ratio as that present in the solid electrolyte. Consequently, the liquid electrolyte consists of a solution of 0.075g THAI and .0075g I_2 per gram acetonitrile. This liquid electrolyte has been shown to exhibit similar performance to the lithium iodide/iodine electrolyte typically used[17].

Photovoltaic Devices:

To make the photovoltaic devices which were tested in this study, $2.5cm^2$ tin-doped indium oxide coated glass (purchased from Delta Technologies, 15-25Ω/cm^2) was cleaned under O_2 plasma (45W, 0.5atm O_2) for three minutes, then washed with

acetone and isopropanol. These were dried in air and masked with cellophane tape (3M "Scotch") along the edges to produce a square well, approximately 1cm^2 in area. If any chemical pretreatment was applied to the cell, it was applied at this point.

Oxide slurry for deposition was made by addition of powdered oxide (nanotubes or Degussa P25 anatase particles) to HPLC grade isopropyl alcohol, followed by vigorous stirring. Isopropanol was one of a number of solvents tested, and provided better film uniformity than ethanol, methanol, or deionized water. The majority of the oxide suspended readily, but the larger aggregates of nanotubes tended to settle out of the slurry. To remedy this, the suspension was allowed to settle, and the material which collected on the bottom was ground with a mortar and pestle and sonicated. The removed material was then added back to the original suspension, and the process was repeated until most of the nanotube material remained suspended when agitated.

For deposition, this slurry was agitated to ensure uniformity. A few drops were added to the center of the tape well on the ITO slide, and a glass stir rod was dragged across the top until the solution was evenly distributed and level with the top of the well. This is typically referred to as a "doctor-blade" film production technique. Films produced by this process were allowed to dry under air flow in a fume hood, at which point they typically formed a solid white film, with visible surface morphology that varied with the concentration of oxide in solution. After drying, any chemical post-treatment was applied and allowed to dry. The tape was then removed and the film placed in an oven and sintered for two hours, typically at 400C although devices were prepared at 300C and 500C as well. This preparation was adapted from several literature sources[3,12,17].

The sintered films were allowed to cool to room temperature. They were then

immersed in a 300μM solution of dye (N719, Solaronix) in anhydrous ethanol (3mL per cell) and left in a sealed, opaque container for 65 hours. They were then removed and rinsed with acetone to remove unadsorbed dye. The edges of the active area were masked with cellophane tape again, redefining a well, which was filled with electrolyte. For the polymeric electrolyte, this was allowed to dry and form a film, which was adhered to a platinum foil by application of a drop of acetonitrile and compression. For the liquid electrolyte, the well was sealed by the application of a platinum foil, ensuring that no bubbles were left inside the well. The platinum foil was large enough to overhang the edge of the cell, allowing a direct electrical connection.

The series of devices manufactured and tested explored the influence of several manufacturing parameters. The effect of oxide film thickness was explored by producing a set of devices following a dilution series, the effect of film bulking treatments was explored by treating the electrodes with titania sol after deposition, and the effect of a blocking layer was explored by treating with sol prior to deposition. Additionally, the effect of sinter temperature (and consequently the crystal phase of the electrode material) was examined.

To explore the effects of serial dilutions and the resulting variation of device thickness, five solvent concentrations were tested. Preliminary investigation indicated that the highest concentration of oxide in isopropanol which would produce an uncracked film with good adhesion to the substrate was about 12.5% oxide by weight. Further samples were made at 8.9%, 7%, 5.7%, and 4.9%. These were all prepared with no additional chemical treatment, and sintered at 400C for two hours.

The impact of sinter temperature was explored by preparation of samples of 5.7% slurry, with no additional chemical treatment. These were treated at 300ºC, 400ºC, and

500ºC and investigated with regards to electrical function, crystal phase of the electrode oxide, and bulk morphology including grain size and porosity.

Chemical treatments were carried out on films prepared from 5.7% slurry. Samples were prepared with an initial layer of titania sol (200mM titanium isopropoxide in ethanol, acidified to pH=1 with glacial acetic acid, added dropwise to fill the tape well) which was allowed to dry before deposition and doctor-blading of oxide slurry. This resulted in a thin, transparent layer of oxide which, it was hoped, would improve contact between the doctor-bladed oxide and the transparent conducting oxide substrate. An additional set of samples was prepared by doctor-blading an oxide layer from slurry, allowing that layer to dry, and adding titania sol dropwise to fill the well. It was hoped that this would improve cell function by bulking the porous oxide and increasing contact between grains of anatase, as titanium tetrachloride is often used to improve device performance[18,19,20], and some reports indicate that titanium alkoxides can produce similar results[21,22]. All chemically treated films were then sintered at 400ºC for two hours.

References:

14. D.V. Bavykin, J.M. Friedrich, F.C. Walsh, *Adv. Mater.*, **18,** 2807 (2006)
15. R. Kawano, M. Watanabe, *Chem. Commun.*,
16. T.M.W.J. Bandara et al, *J. Solid State Electrochem.*, **14**, 1221 (2010)
17. Y. Ohsaki et al, *Phys. Chem. Chem. Phys.*, **7**, 4157 (2005)
18. P. Charoensirithavorn et al, *J. Electrochem. Soc.*, **157**, B354 (2010)
19. P. Tiwana et al, *J. Phys. Chem. C.*, **114**, 1365 (2010)
20. D. Zhang, Y. Liu, W. Wang, X. Xiao, *Chinese Science Bulletin*, **45**, 1956 (2000)
21. D. Menzies et al, *J. Aust. Ceram. Soc.*, **39**, 108 (2003)
22. M. Zukalova et al, *Nano Lett.*, **5,** (2005)

Characterization of Devices

Electrical Characterization

Electrical characterization and measurement of a series of optical devices has been a crucial part of this investigation. Preliminary devices were characterized by IV measurement and time dependent short-circuit current measurements taken under regulated illumination provided by a halogen source (irradiance kept constant but not measured). Measurements on the final devices were made by current/voltage measurement under a regulated, 1sun, 1.5 air mass source. The same series of devices was also characterized by IPCE, with a monochromator, mercury vapor source and a silicon reference photodiode.

The initial IV measurements were made using a Keithley 4200-SCS semiconductor characterization system, in two-probe mode. The built in "Solar Cell" program was used to run forward and reverse bias sweeps, and to monitor current under no bias. One-sun IV measurements were made on a computer system consisting of a LabView module acquiring data from a Keithley 2400 Digital SourceMeter, while IPCE measurements were made through a Keithley 6517 high resistance electrometer (IPCE and IV measurement equipment made available by UNC EFRC).

Optical Characterization

Optical measurements were used to determine the absorption spectrum of dye-loaded oxides, as well as to ascertain crystal phase. The techniques used were UV-visible spectroscopy, using a Cary 400 UV-Visible spectrophotometer, and Raman

spectroscopy, with the excitation provided by an Ar^+ laser providing ~100mW at 514nm, focused on the sample in micro-Raman configuration.

UV-Visible spectra were measured to determine the absorption spectrum for the N719 dye used in this study, both in ethanol solution and adsorbed on titania. This technique was further used to compare the dye loading per unit mass between the two primary oxides. Specifically, doctor-bladed films deposited from isopropanol suspension of either anatase or nanotubes were sintered and weighed on a scale accurate to 0.1mg. Each was then submerged in a precisely-known mass of ethanolic N719 solution at molarity determined by UV-Vis. These films were allowed to sensitize for 18 hours, and the remaining solvent was measured under UV-Vis to determine remaining concentration of the dye. This measurement was repeated at 65 hours.

Raman spectroscopy was used to discern between anatase, nanotube, and TiO_2-B phases (and mixtures thereof) in doctor-bladed electrode films subjected to thermal and chemical treatments.

Microscopy

Both optical microscopy and scanning electron microscopy were employed as surface characterization techniques, and for the assessment of film quality. SEM was performed on a Hitachi S-4700 SEM (UNC CISMM); optical microscopy was performed on a Nikon Eclipse LV-150 binocular microscope (UNC CHANL).

III: Data and Results

Raman Spectra

There are a number of trends which can be readily discerned from the data collected in this study. Concentration, electrode material, electrolyte type, thermal and chemical treatment have all been examined, and are related to trends in properties of the final device or some part thereof. In particular, the data from Raman, SEM, and IV will be examined as they relate to the effects of these parameters, their consequences, and how they influence

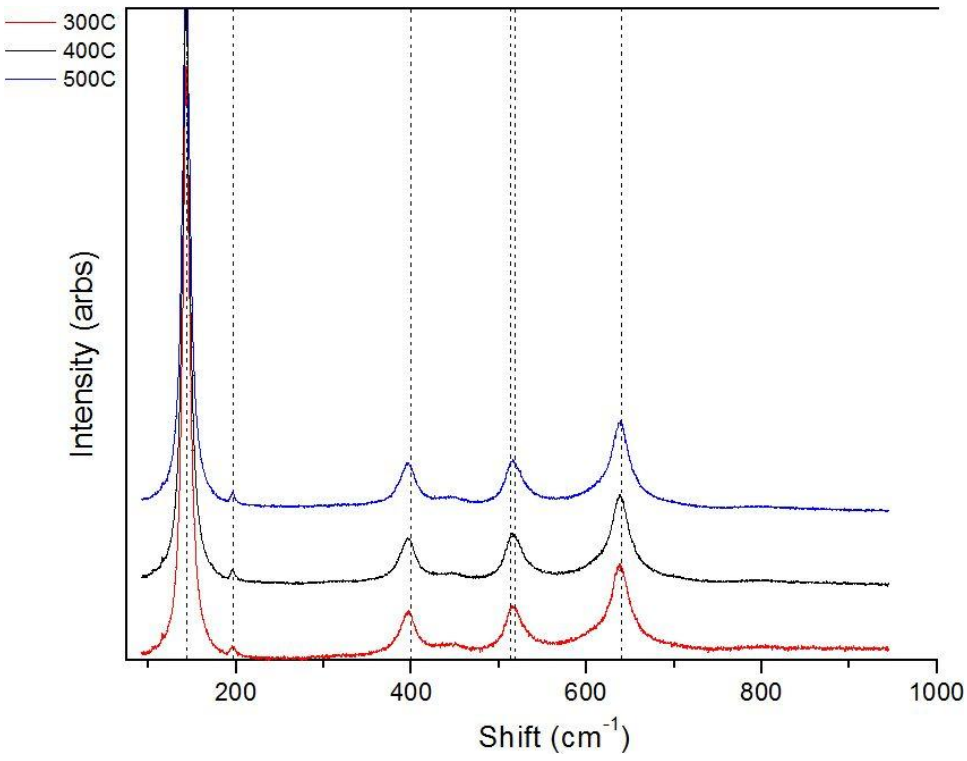

Figure 6: Raman spectra of heat-treated anatase film. Dashed vertical lines show peaks characteristic of anatase.

one another.

The first parameter to be examined is the effect of thermal treatment on the two starting phases of titania. Electrodes made from both anatase and nanotube titania were treated at 300, 400, and 500ºC and observed under Raman spectroscopy. From the resulting spectra (figures 6 and 7), it can be seen that the sol-treated nanotube-based electrodes display peaks characteristic of both anatase and nanotubes, with the nanotube peaks becoming increasingly suppressed with increased treatment temperature, so that even at 400ºC, the nanotube character of the film is so reduced that only the peak at 480cm^{-1} remains clear. For the electrodes which began as anatase, little in the way of thermal alteration can be seen. The only peaks appearing in the spectra are those characteristic of anatase.

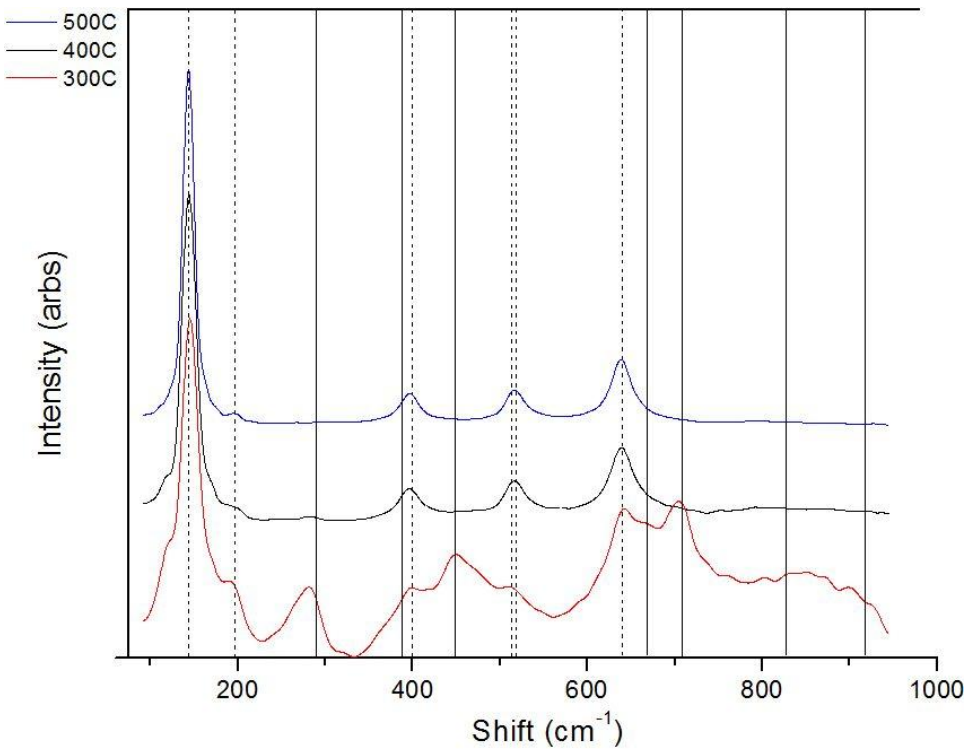

Figure 7: Raman spectra of heat treated nanotube and sol film. Dashed vertical lines show peaks characteristic of anatase, while solid lines show nanotube peaks.

It seems clear from these results that electrodes treated at 400ºC or higher are at least mostly composed of anatase. The other parameter which has the potential to impact crystal phase is the application of titanium isopropoxide, which is expected to contribute to film connectivity by depositing anatase of ~5nm grain size and increasing "necking" between grains in contact[17]. Examining the nanotube and anatase films, it can be seen that the sol-treated anatase film is indistinguishable from the untreated film, while the sol-treated nanotube film has suppressed nanotube peaks after heating as compared with the untreated film (figure 8).

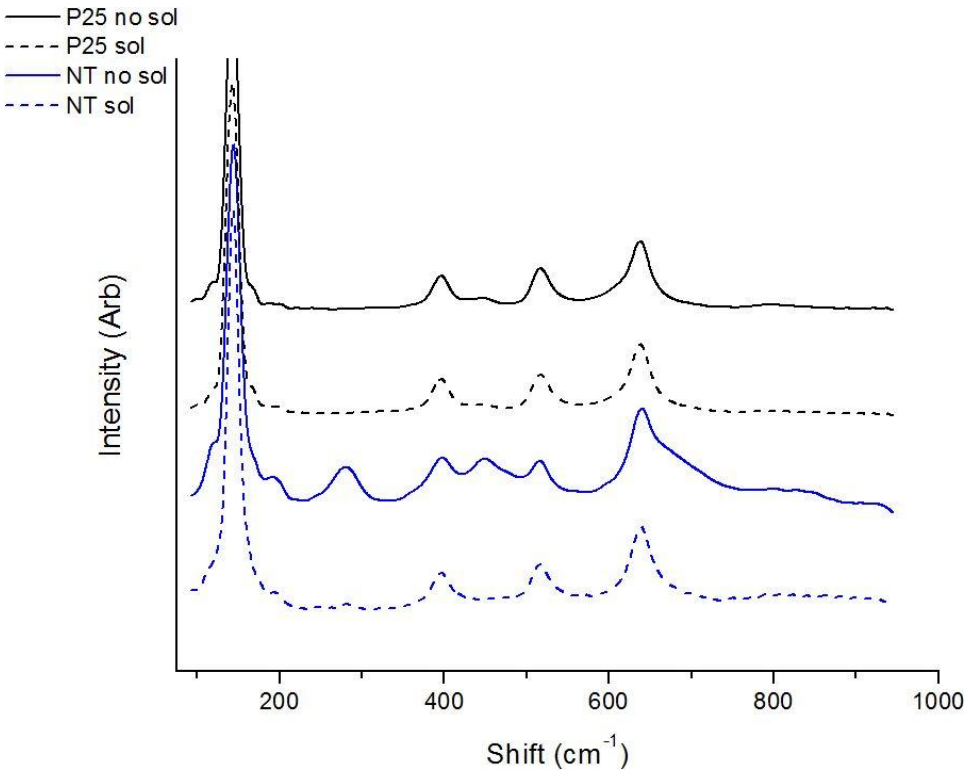

Figure 8: Raman spectra from untreated and sol treated films of anatase and nanotubes, all sintered at 400°C.

Scanning Electron Micrographs

Despite the minimal difference in crystal structure from starting material, further examination indicates that there are still significant differences stemming from the use of anatase or nanotubes in electrode deposition. Scanning electron micrographs of both types of electrodes indicate differences at the micro- and nanoscale, with nanotube electrodes retaining the micron-sized aggregates of rod- or tubelike structures characteristic of as-synthesized nanotubes, and anatase electrodes developing a foamy, porous structure.

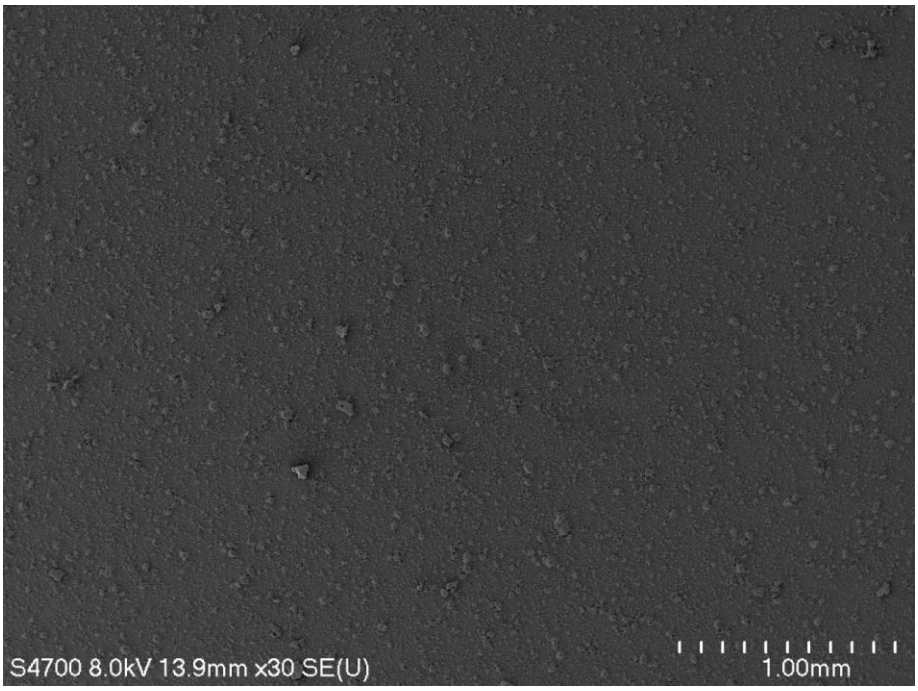

Figure 9: SEM at 30x, Nanotube film. Note that at this scale, film is level and smooth, comparable to anatase film, except for 50-100µm aggregates.

The apparent similarity of the films at optical scales breaks down quickly as the magnification is increased. While both are fairly regular at the millimeter scale, differences emerge when features with ~10µm size can be resolved. At that point, it is clear that the nanotube films are primarily composed of aggregates with size on the order of a few

microns to a few tens of microns, packed into a layer with 1-10µm gaps between the aggregates. At the same scale, the anatase films appear relatively continuous, with the layer apparently divided into plates ~100 µm wide, separated by 1-10µm cracks.

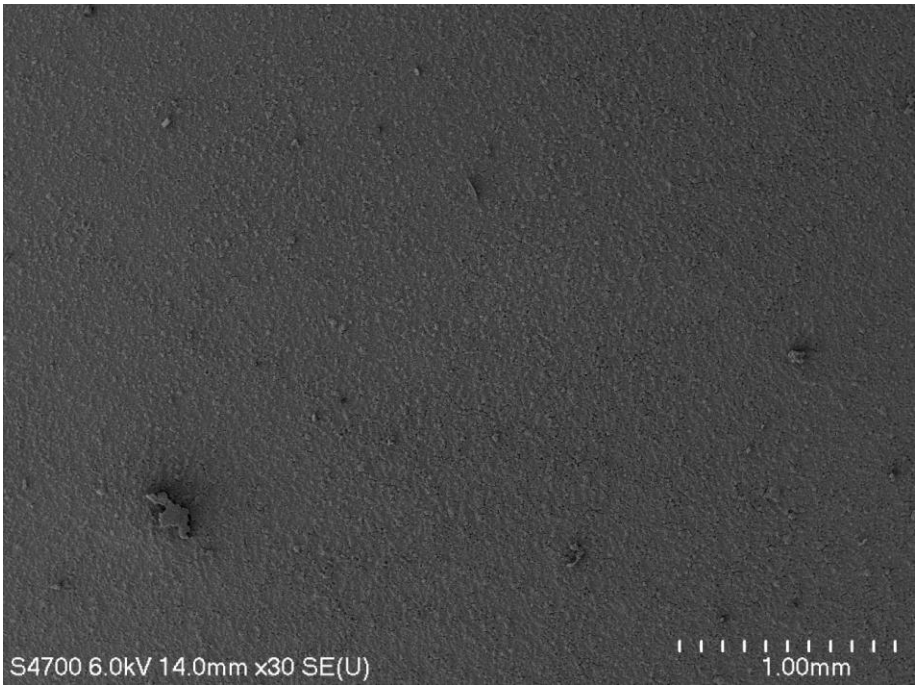

Figure 10: SEM at 30x, Anatase film. Note the lack of large aggregates compared to the nanotube

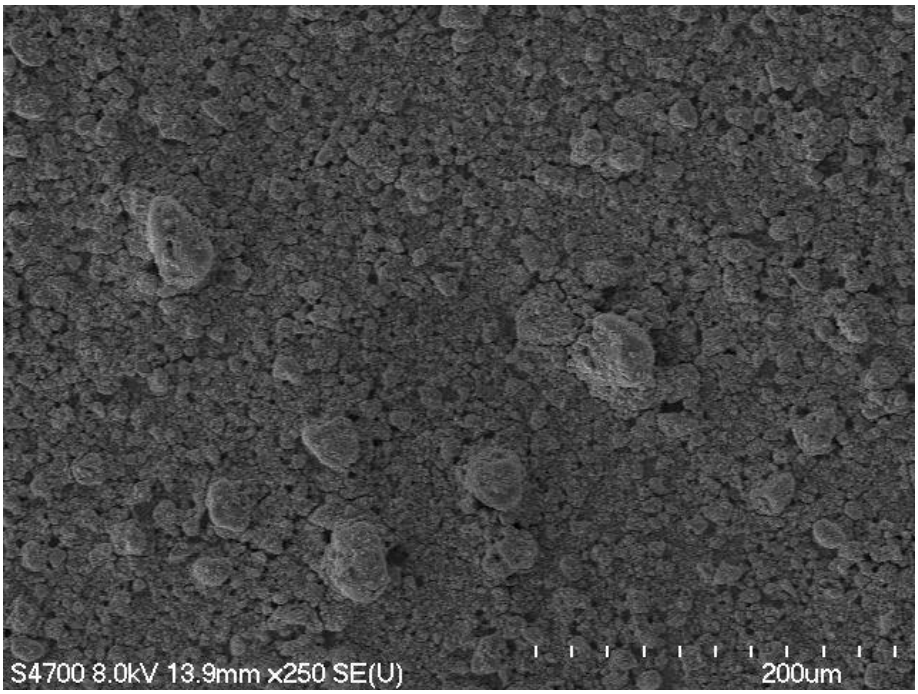

Figure 11: SEM at 250x, Nanotube film. At this scale, the "gravel pile" nature of the film begins to become apparent.

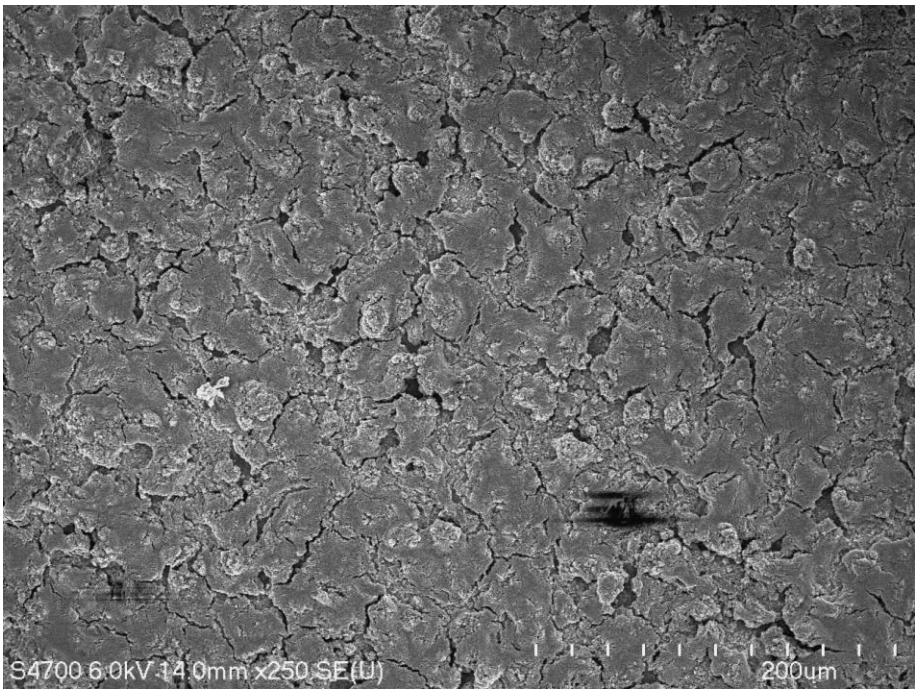

Figure 12: SEM at 250x, Anatase film. Compared to the nanotube film, it's clear that these films are more monolithic and interconnected.

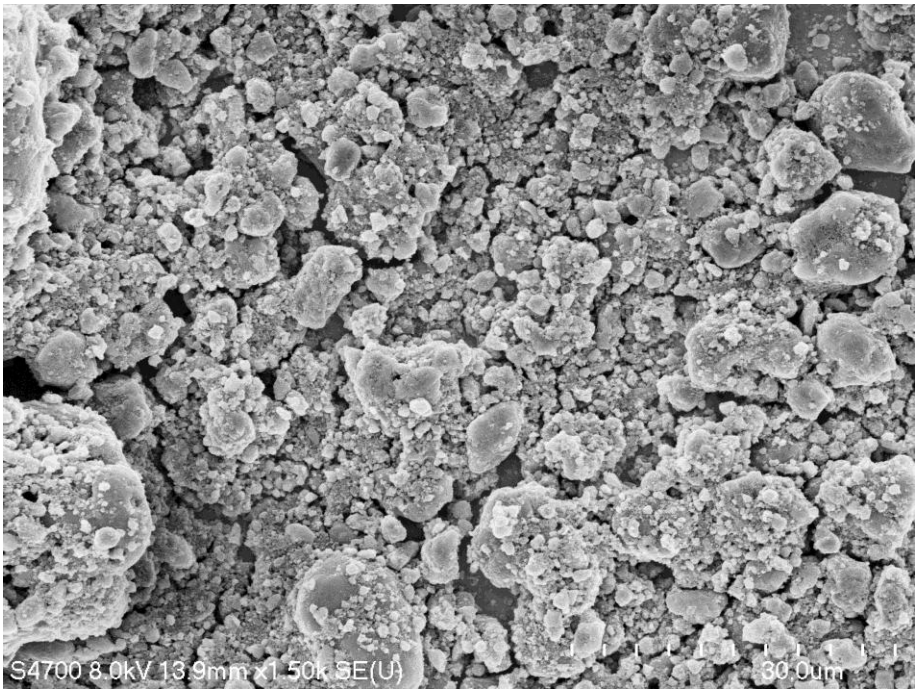

Figure 13: SEM at 1,500x, Nanotube film. Voids in the film are plainly visible, between the aggregates which make up the body of the film.

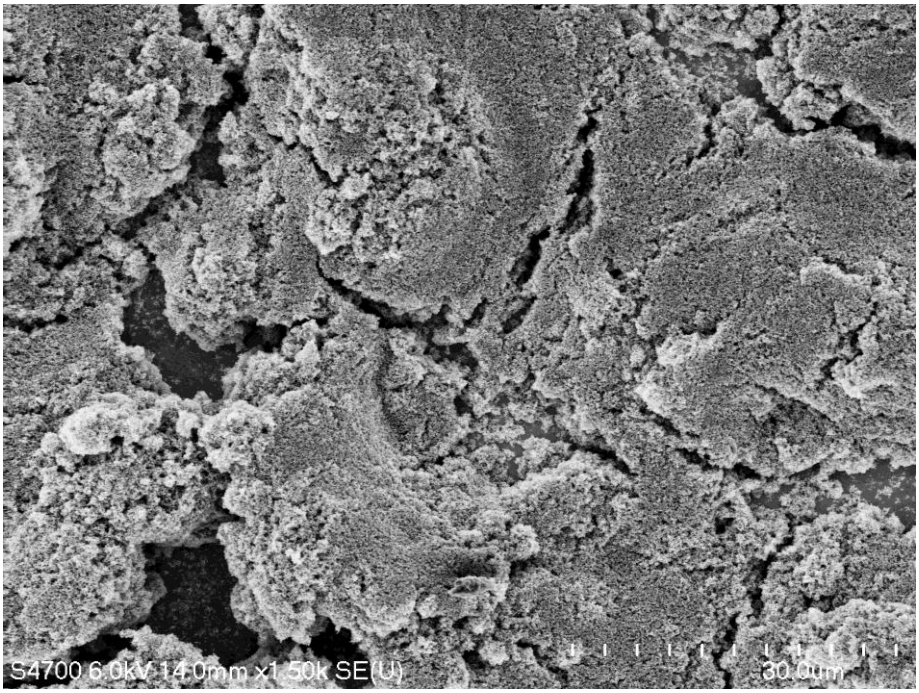

Figure 14: SEM at 1,500x, Anatase film. Much more continuous than the nanotube film, the pores in the volume of the material are visible at this scale as well.

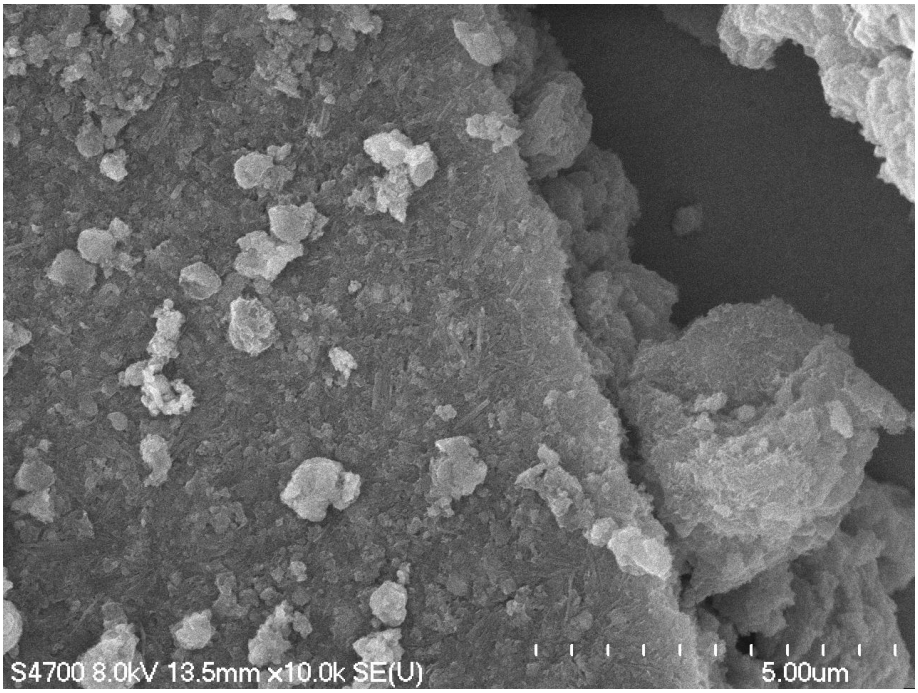

Figure 15: SEM at 10,000x, Nanotube film. At this scale, the reduced porosity is extremely clear, and the sheetlike crystals resulting from breakdown of nanotubes can be seen.

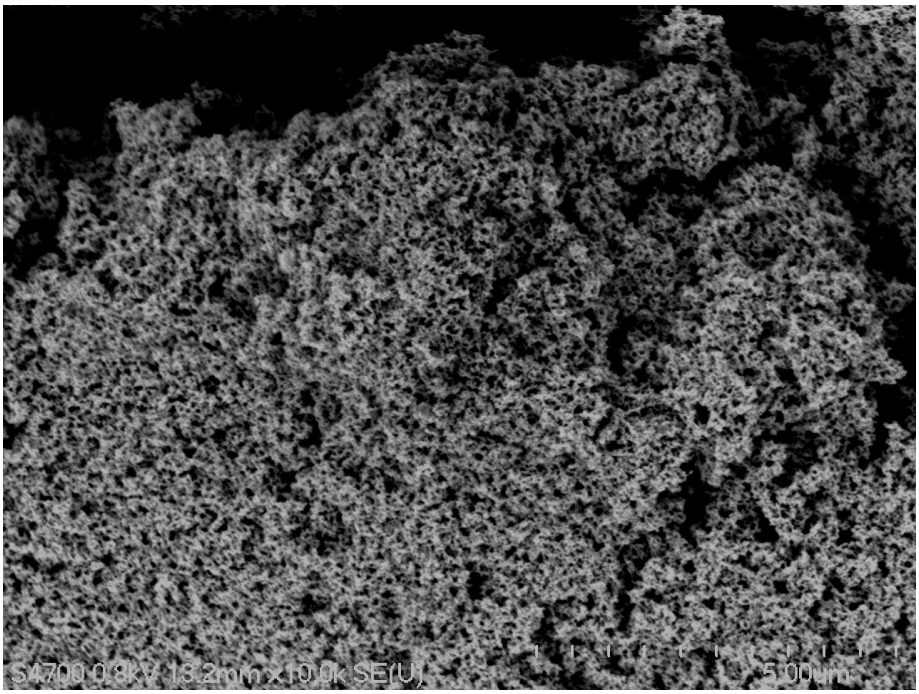

Figure 16: SEM at 10,000x, Anatase film. Pores with ~10nm size can be seen, but the individual crystallites are still too small to resolve.

Figure 17: SEM at 35,000x, Nanotube film. Very little in the way of discernible pores, but the quasi-1D crystallites are easily seen at this scale.

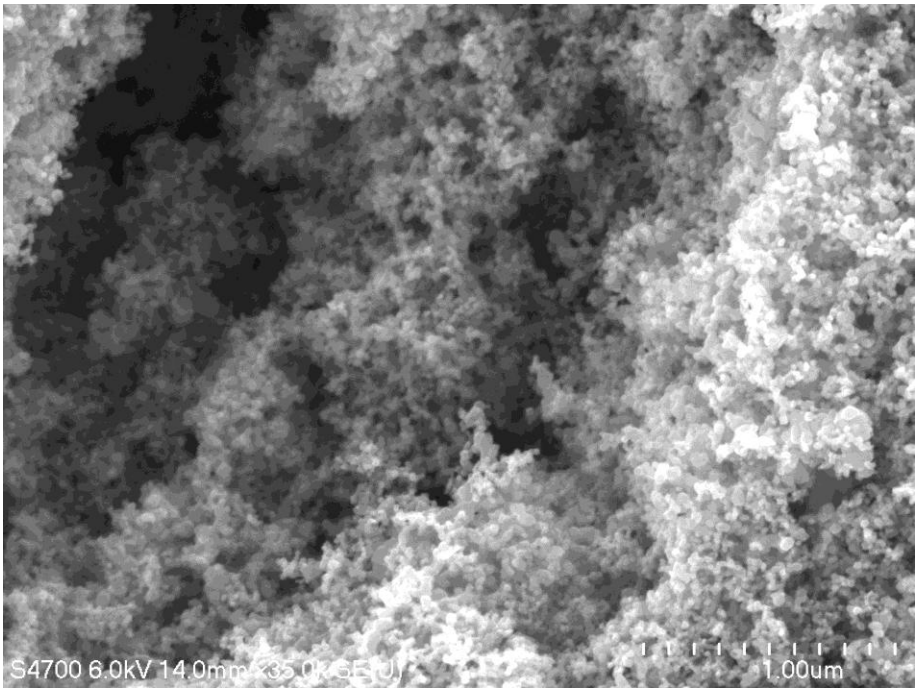

Figure 18: SEM at 35,000x, Anatase film. Crystallites are first visible at this scale, the filamentary structure is apparent, and the pores of 10-100nm are clear as well.

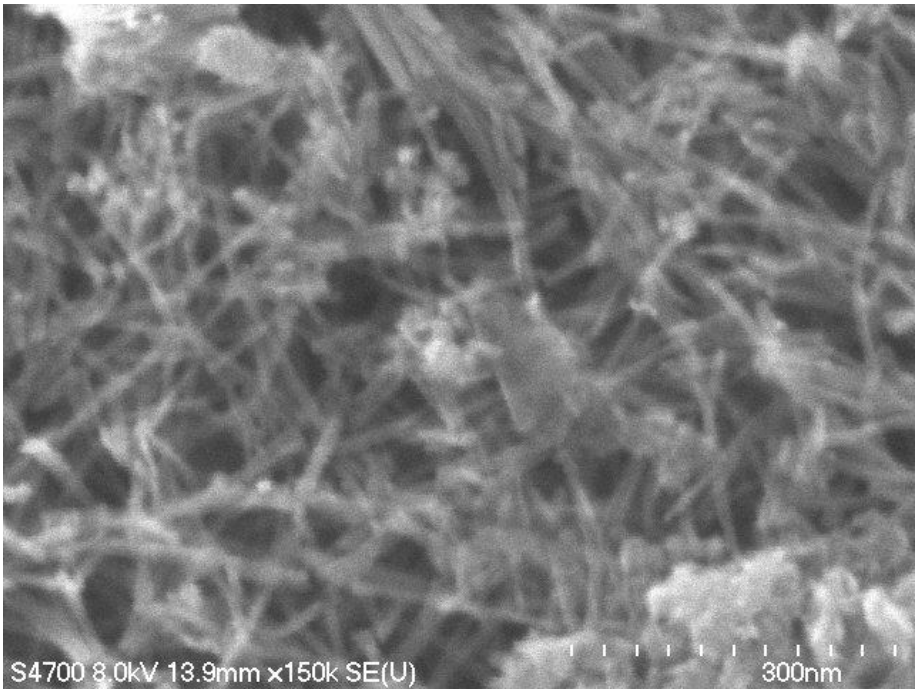

Figure 19: SEM at 150,000x, Nanotube film. A highly "tubey" region of a nanotube film. Even when sintered, some regions retain a nanotubular or nanowire morphology, particularly near creases and depressions in the aggregates visible at larger scales.

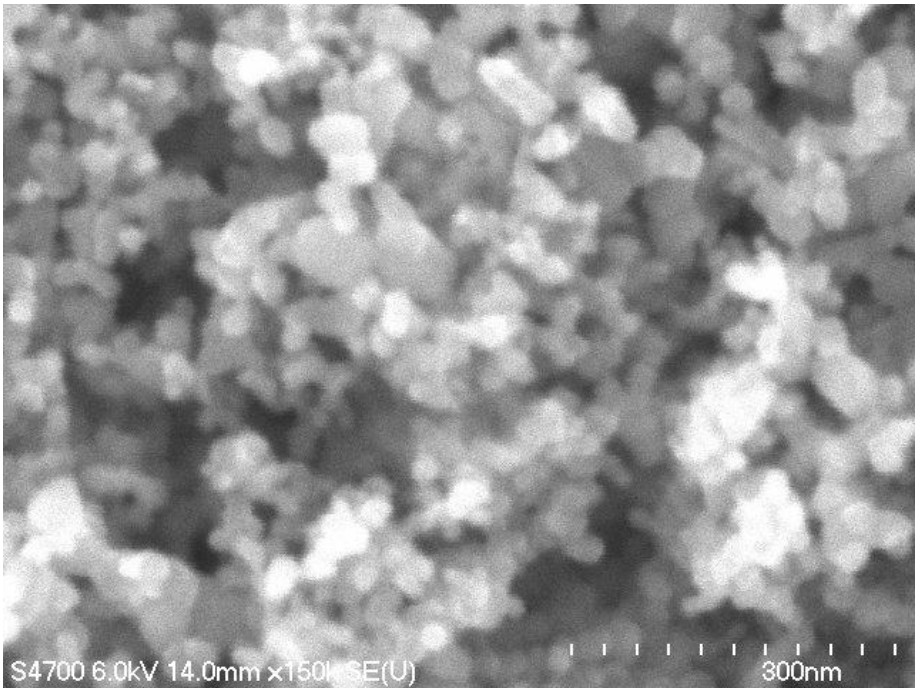

Figure 20: SEM at 150,000x, Anatase film. Crystallite size can be seen clearly here, as can all pore scales.

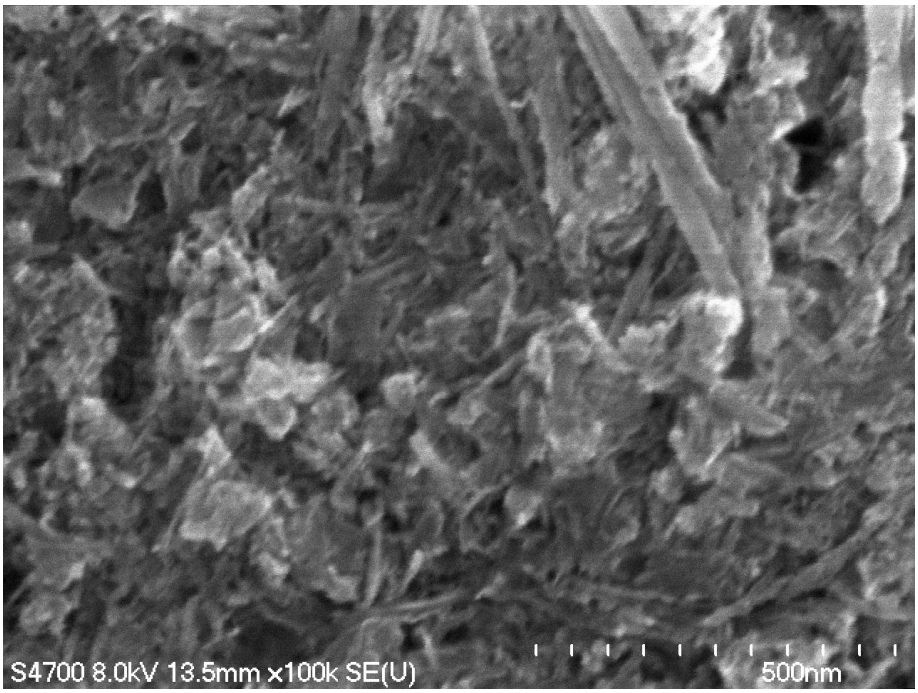

Figure 21: SEM at 100,000x. Sintered nanotube film, showing low porosity and densely packed, quasi-1D crystallites. Compare to figure 17.

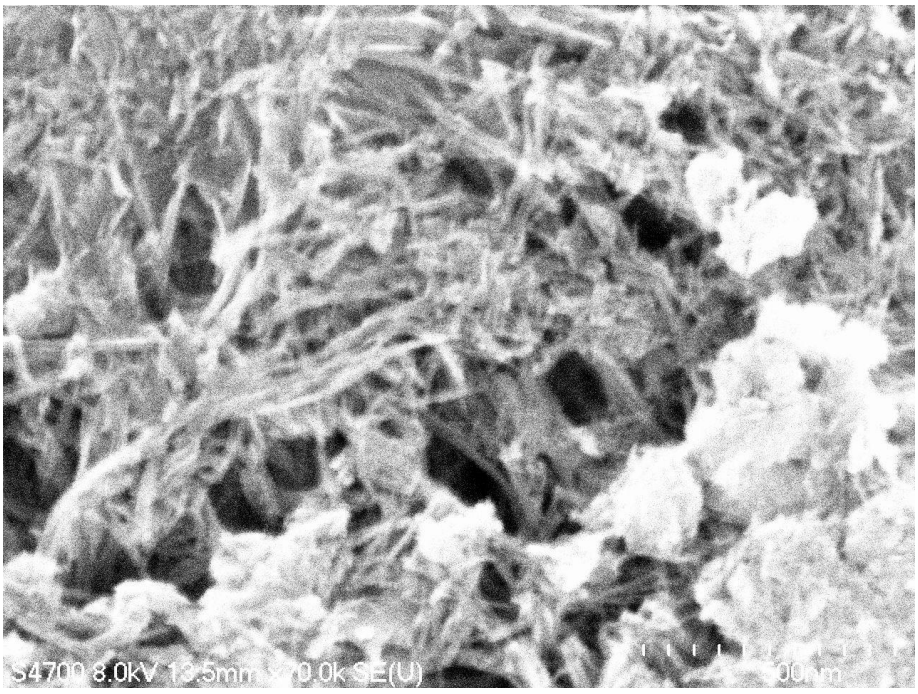

Figure 22: SEM at 70,000x, Unsintered nanotube film. Note the entangled tubes with much greater porosity than the sintered film.

When features of several tens of nanometers can be resolved, the porosity of the anatase films becomes readily apparent, as they form a foam-like network which appears to be continuous, with pores of 10-100nm. At this same scale, the nanotube films can be seen to pack very densely, with quasi-one-dimensional crystallites visible in the aggregate material. The sintered nanotube material appears to be mostly monolithic at this scale, lacking the pore structure apparent in the anatase. Some regions of the nanotube films exhibit higher porosity, as shown in figure 19, these mostly occur around creases in the aggregates. The anatase nanoparticle films also exhibit porosity on the scale apparent at 150kx, showing pore structure as small as 3nm.

Samples of blended polymer electrolyte and oxides were also examined under SEM, to determine the degree of blending of the polymer into the oxide pores. Regions where the oxide films crack under strain allow for assessment of the degree to

which the electrolyte has infiltrated the oxide. From examining these regions, and from examining the magnification levels at which pores would be apparent, the degree of blending and pore-filling can be assessed.

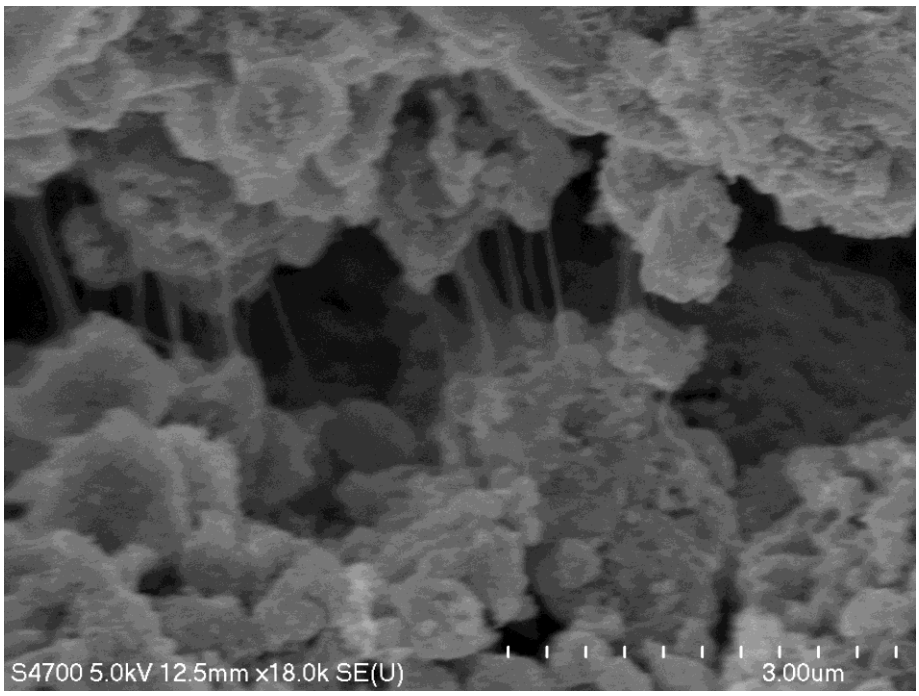

Figure 23: SEM at 18,000x, Nanotube film. Polymer filaments bridging a crack in the film can be seen here. Note scale as compared to anatase film.

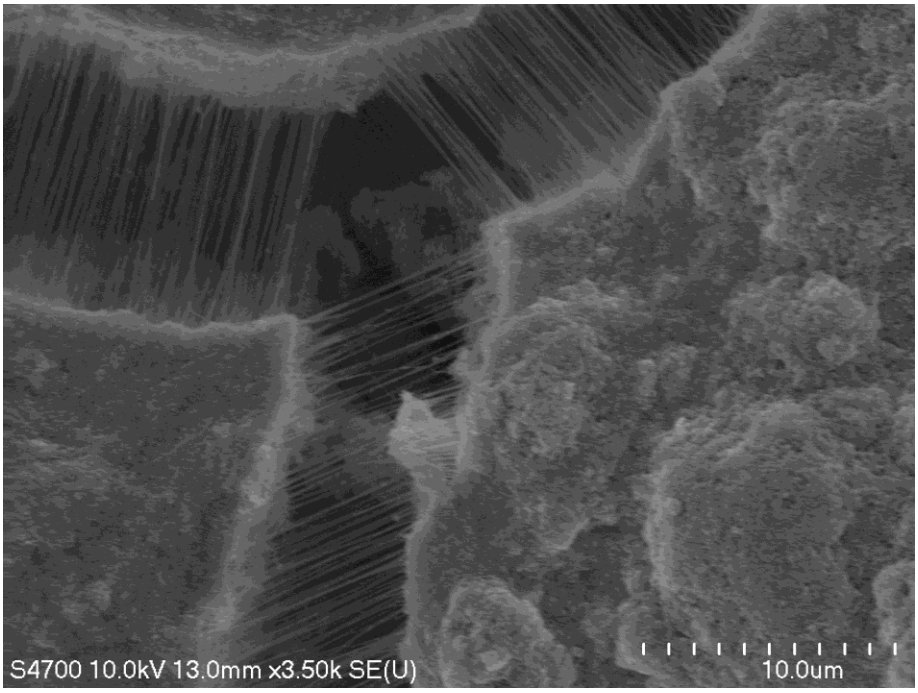

Figure 6:SEM 3,500x, Anatase film showing polymer filaments near crack in film. Anatase shows more polymer bridging gaps, and more filling of surrounding region.

Notable differences in the nanotube films were also seen for treatment with titanium isopropoxide after film deposition. Films for imaging were prepared as described under the experimental section with a titanium isopropoxide post-treatment, and then allowed to dry under air flow in a fume hood. Differences in porosity are readily apparent on the same scale that porosity differences are apparent in the untreated films. The application of titania sol to the nanotube film appears to reduce the porosity even further by filling in all but the largest pores, producing a monolithic layer of titania with quasi-one-dimensional rodlike structures visible embedded in the surface.

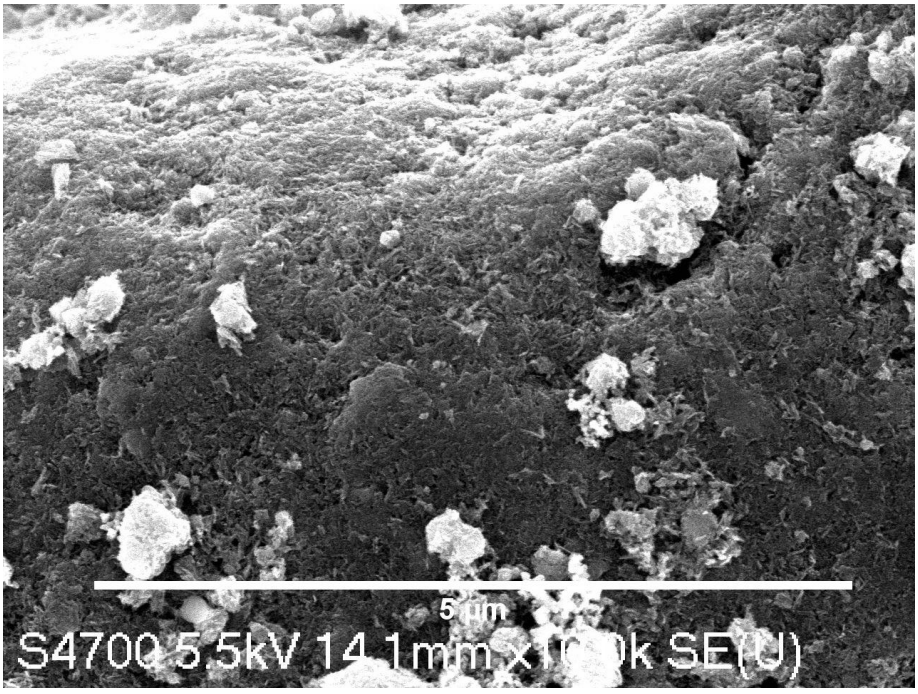

Figure 25: SEM at 10,000x. Sintered nanotube film, without isopropoxide treatment. Porosity is low but discernible, 1-d crystallites are visible as well.

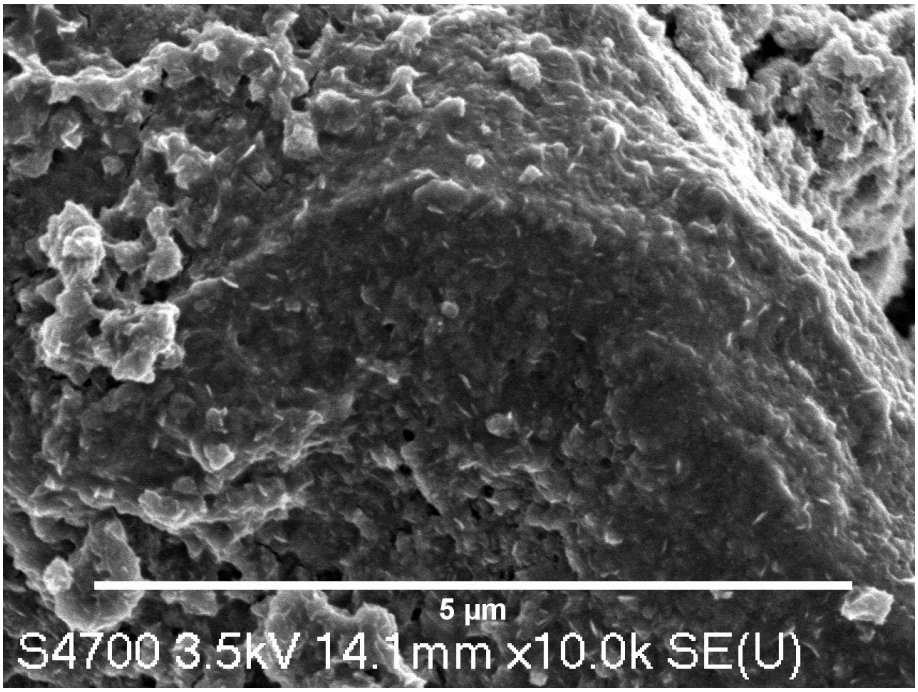

Figure 7: SEM at 10,000x, Sintered nanotube film with isopropoxide treatment. Note further reduction in porosity from the untreated film, as well as greater connectivity. 1D crystallites are still visible embedded in filler material.

Current-Voltage Measurements

Differences in function depending on manufacturing parameters are most clearly evident from measurement of current as a function of bias voltage, under illumination and in the dark. This allows the determination of the internal parameters of the diode circuit model as discussed above. For this set of experiments, the devices were assembled and clipped into a PTFE holder which held the layers (the platinum foil and device with a tape-masked well containing liquid or polymer electrolyte) together for the duration of the experiment. This allowed for a compromise between durability and reusability, so that the same devices tested with liquid electrolyte could be rinsed and reused with solid electrolyte, allowing comparison on a more even basis. The data collected allow comparison across all varied parameters.

From the dark and illuminated JV curves (IV curves scaled by device area to yield current density), a number of the important parameters describing the function of a solar cell can be determined. The open circuit voltage and short circuit current (V-intercept and J-intercept, respectively) can be found directly from the plot measured under illumination. An approximate value for the shunt resistance can be obtained from the reverse-bias dark JV curve, where the inverse slope of the linear region near the intercept in the third quadrant (figure 27) gives an approximate value of R_{sh}. The inverse slope of the illuminated curve at the V-intercept can be taken as proportional to the series

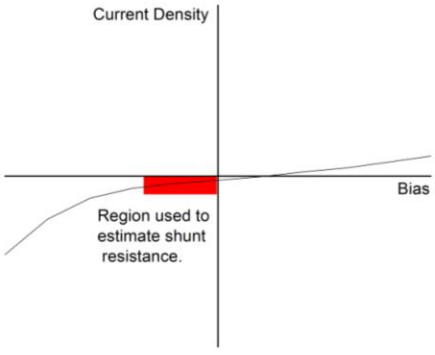

Figure 8: Linear extrapolation of red boxed region of curve provides estimate of R_{sh}.

resistance, although the value obtained is not accurate enough to be called an estimate, particularly for devices far from ideal diode behavior. By calculating the maximum power in the illuminated JV curve, the device fill factor (defined as the ratio of $P_{max}/V_{oc}J_{sc}$) can be calculated, allowing a comparison to a hypothetical equivalent ideal device (which would have a fill factor approaching 1).

Film thickness was the initial parameter subject to variation, as the initial doctor-bladed films were prepared in very small batches as a proof of concept, and performance was noted to vary with some dependence on the concentration of the deposition slurry. It was experimentally determined that the highest solvent-to-oxide ratio which would result in a continuous, adhering film was 8:1 by mass. The solvent concentration was increased stepwise from that level, producing a set of devices of varied thickness. Ultimately, devices were produced and tested at 12.5, 8.8, 7.0, 5.7, and 4.9 percent oxide by weight. Devices were produced at 2.5 and 1.3 weight percent as well, but the consistency was low and a large number of the devices were defective; consequently the results of those tests have not been included. All devices in this set were sintered at 400C and received no chemical treatment.

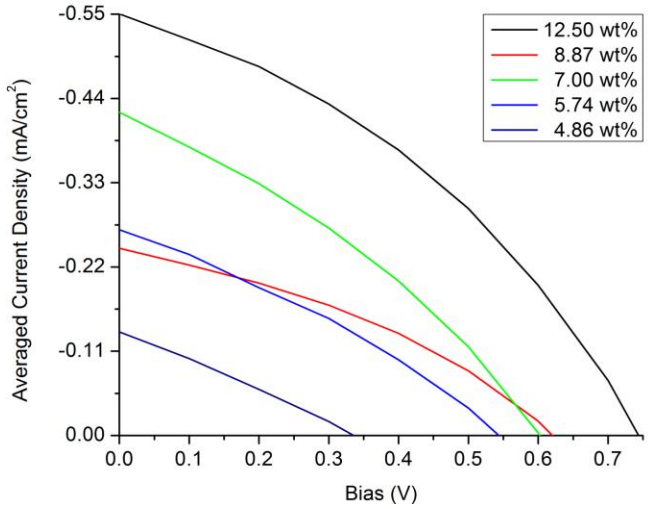

Figure 9: Average over nanotube and anatase devices, both electrolyte types, dependence of JV curve on deposition concentration.

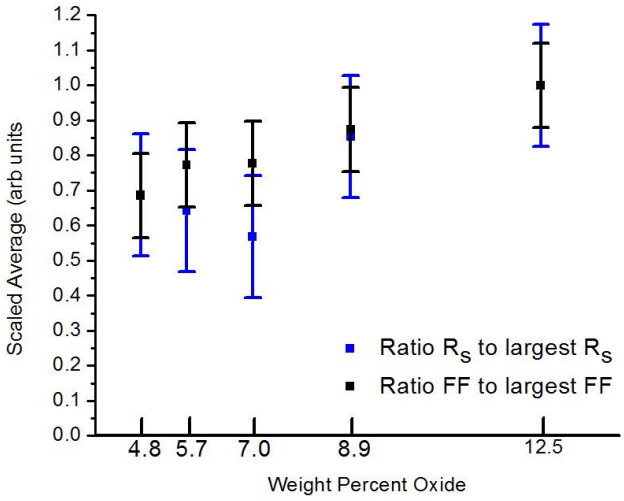

Figure 10: Shunt resistance and fill factor (both scaled 0-1) dependence on oxide percent, averaged over all other factors.

Another parameter subject to experimental variation was the temperature at which the sinter process was conducted. For each combination of electrode and electrolyte, a sample was prepared by a 300, 400, and 500C two-hour sinter process. All temperature variation samples were made with a deposition solution of 5.74wt% oxide and no chemical treatment.

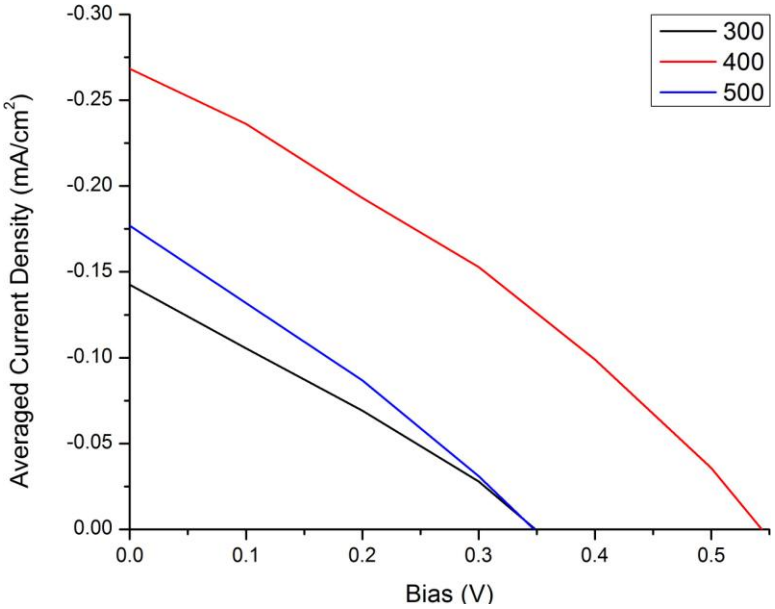

Figure 30: Average over nanotube and anatase devices, dependence of JV curve on sinter temperature.

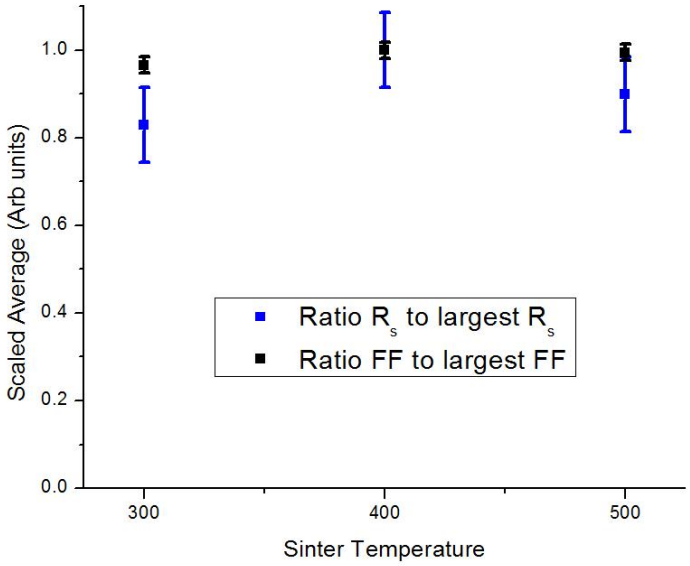

Figure 31: Shunt Resistance and fill factor (both scaled 0-1) dependence on sinter temperature, averaged over all other factors.

Chemical treatment was also explored as a parameter. A 2 millimolar solution of titanium isopropoxide in ethanol, with acetic acid to lower pH to 1 was added in three treatment types: pre-treatment in which bare ITO was treated with isopropoxide sol to form a blocking layer, post-treatment in which a dried oxide film was treated with isopropoxide sol to bulk the film and improve connectivity, and both. All films were prepared from the 5.74wt% solution, and sintered at 400C.

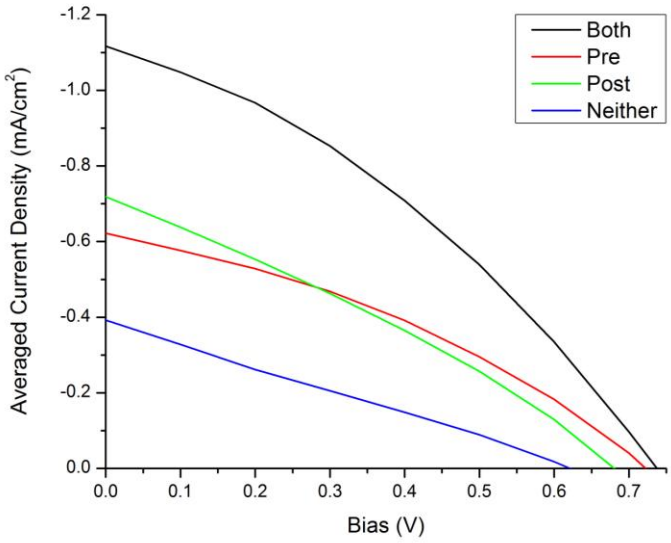

Figure 32: Average of anatase and nanotube devices, both electrolytes. Dependence of JV on chemical treatment.

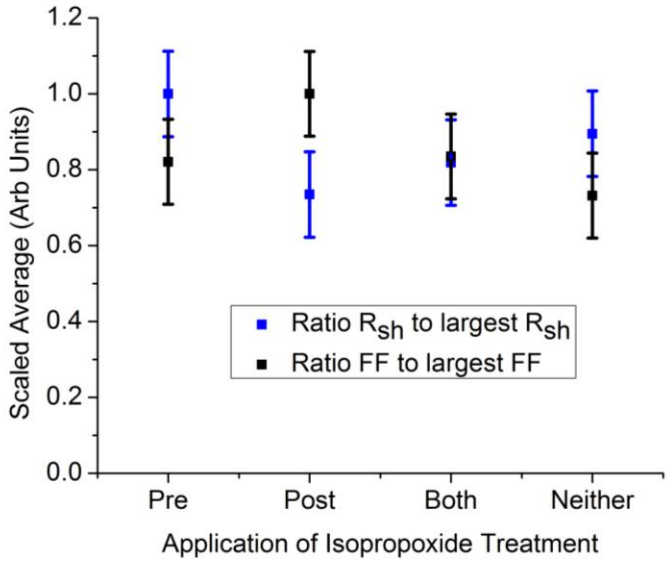

Figure 33: Shunt resistance and fill factor (both scaled 0-1), dependence on chemical treatment. Averaged over all other factors.

The final two parameters are the starting structure for the oxide electrode, and the electrolyte material (plasticized PEO solid, or acetonitrile liquid solution). These will be treated together, as there is interaction between the effects of varying those parameters. The compound effects of varying other parameters will be examined in conjunction.

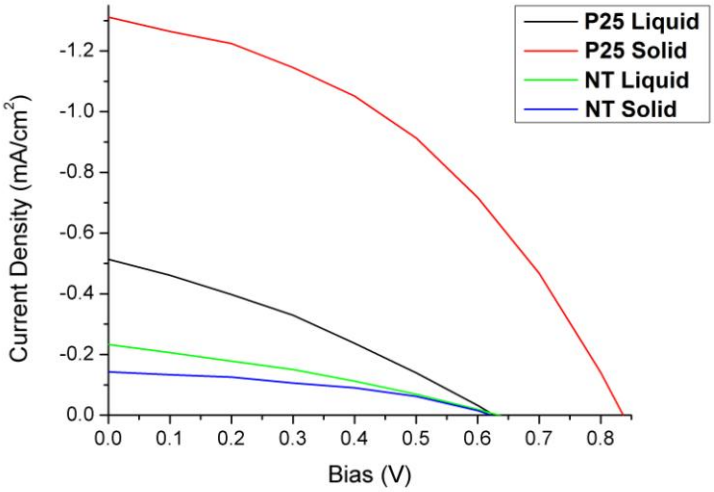

Figure 11: Comparison of devices made with 12.5 wt% oxide, 400C sinter, and no chemical treatment.

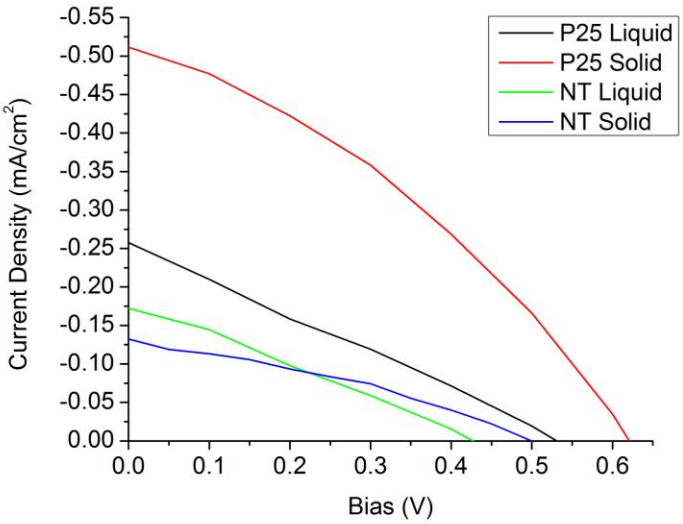

Figure 12: Comparison of devices made with 5.74 wt% oxide, 400C sinter, and no chemical treatment.

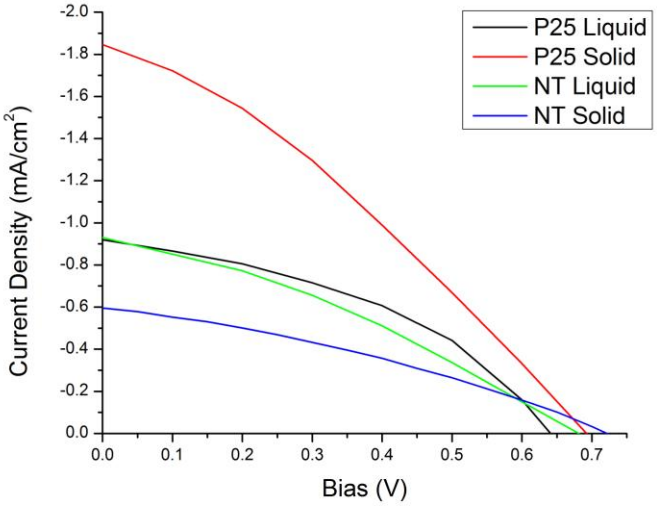

Figure 13: Comparison of devices made with 5.74 wt% oxide, 400C sinter, and isopropoxide pre- and post-treatment.

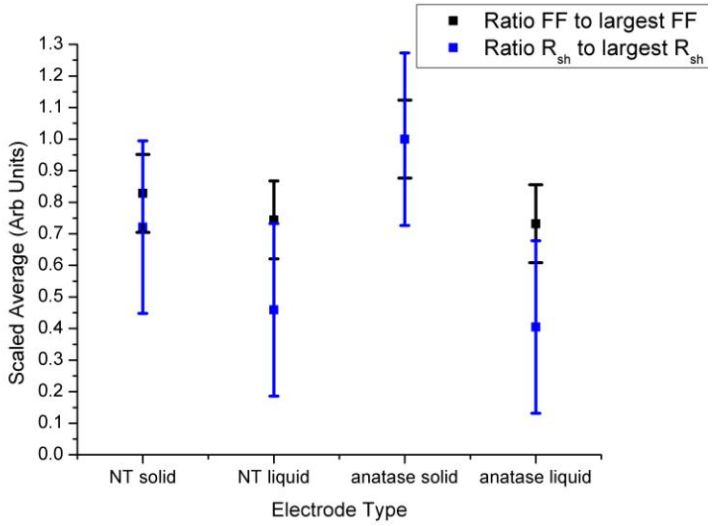

Figure 14: Shunt and fill factor (scaled 1-0), dependence on electrode and electrolyte. Averaged over all other factors.

There are a number of interesting phenomena and general trends which are apparent from the illuminated current-voltage data, in combination with the fill factor and shunt resistance data. The dependence of device properties on preparation parameters is primarily interesting for optimization purposes, as there is a weak correlation between fill factor and concentration of oxide in the deposition slurry. Increasing concentration also shows a weak correlation to shunt resistance, Voc and Jsc, at least to the extent that the thickest films show the largest values of those parameters. Processing temperature shows a stronger correlation to all parameters, with a process temperature of 400C resulting in optimal performance. The correlation to fill factor is relatively weak, while open circuit voltage and short circuit current are significantly improved at 400C as compared to 300 or 500C, and the improvement to R_s is visible from both the IV plot and the plot of average resistance.

The chemically-treated films show a strong dependence on treatment, with pre- and post-treatment producing similar results on the JV curve, and a combination of the two

treatments producing the greatest impact on open circuit voltage and short circuit current. Fill factor and shunt resistance appear to be affected to a similar degree, but in a surprising fashion: application of a pretreatment produced little apparent difference from the untreated films. Post-treatment appears to improve fill factor at the cost of shunt resistance, and the application of both treatments appears to slightly improve fill factor, while slightly reducing shunt resistance.

The interaction of the choice of electrolyte with choice of electrode material was unexpected, but the outcome was consistent, regardless of the state of the other parameters. This is particularly interesting when the effect of switching to the polymer electrolyte is compounded with parameters which otherwise improve device performance, namely increasing film thickness and applying a film-bulking chemical treatment.

For the anatase films, use of polymer electrolyte results in the improvement of short circuit current and open circuit voltage in all cases (although the V_{oc} improvement is less notable in the isopropoxide treated film). The fill factor and shunt resistance also see significant improvement. The nanotubes do not see a corresponding improvement to their JV performance under 1 sun illumination. In fact, in all cases examined, the short circuit current with the solid electrolyte was reduced from the baseline measurement made with the liquid electrolyte. Open circuit voltage typically saw a slight increase as compared with the liquid electrolyte, particularly when combined with isopropoxide chemical pretreatment. Both fill factor and shunt resistance improved, but not to the extent that they improved for the anatase devices.

Photon-to-Current Efficiency

In order for a solar cell to be said to function well, it must demonstrate useful power conversion efficiency. As mentioned in the introduction, current top-performing DSSC devices achieve roughly 10% efficiency over the visible spectrum. The cells produced in this study do not approach this efficiency, but efficiency measurements still provide a great deal of information about the function of the device, providing another parameter for comparison between differently-manufactured devices.

In this study, incident-photon-to-current efficiency (IPCE) was determined by comparison of the wavelength-dependent photocell current to the power spectrum determined for the source by a calibrated silicon detector, according to the equation:

$$\eta_{IPCE}(\lambda) = \frac{1240 * I_{sc}(\lambda)}{\lambda * P_{photo}(\lambda)}$$

where I_{sc} is the output current from the cell under zero load and P_{photo} is the power as determined by the silicon detector. This wavelength dependent representation of device efficiency is useful for comparison to the absorption of the materials which make up the photocell (figure 33 shows sensitized anatase and nanotube film UV-Vis absorption).

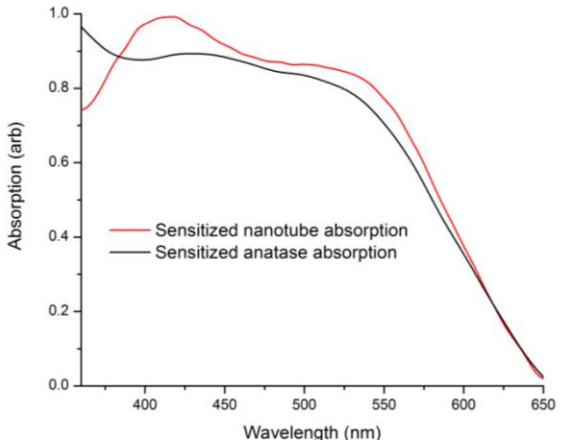

Figure 15: UV-Visible absorption for sensitized anatase and nanotube films for comparison.

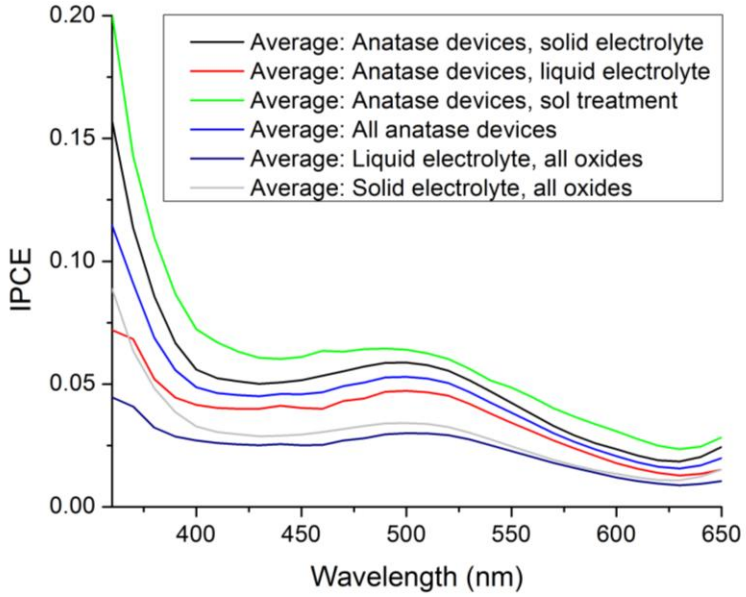

Figure 16: Averaged IPCE curves for anatase devices prepared under varied electrolyte and chemical treatment conditions. Average of all liquid and solid electrolyte devices provided for comparison.

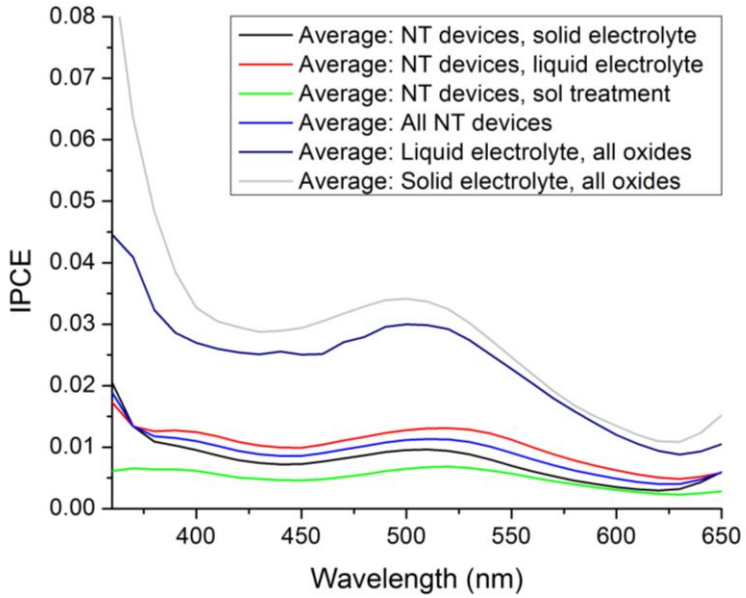

Figure 40: Averaged IPCE curves for nanotube devices prepared under varied electrolyte and chemical treatment conditions. Average of all liquid and solid electrolyte devices provided for comparison. Note reversal of treatment effect on efficiency as compared to anatase devices.

From the IPCE data, the difference in power generation between the electrode materials can be better described. It is clear that despite the uniformly-lower conversion efficiency of the nanotube devices, the spectra are similarly shaped, with corresponding peaks.

The effect of parameter variation can also be understood better through examination of the changes to the IPCE. In the samples examined for IPCE, chemical treatment was applied in the form of titanium isopropoxide sol applied dropwise after deposition of the standard oxide film (5.4wt% oxide). The resulting films were sintered at 400C. The visible result of this is a substantial gain of efficiency for anatase devices. The curve shown displays the effect of the treatment averaged over solid and liquid electrolytes, with an improvement effect more significant than that shown in the average solid electrolyte device. Conversely, performance is substantially degraded in the nanotube devices when they are treated with sol. In fact, where the sol-treated anatase films are the most effective class of devices, sol-treated nanotube films are the least effective class overall, with even the efficiency maximum returning less than 1%.

A similar effect is clear for the use of solid electrolyte. Averaged over all other factors, solid-electrolyte anatase devices are the second most efficient class of device, while the solid-electrolyte nanotube devices are the second worst. The gain in performance by the anatase devices is enough that when electrolyte type is examined over the average of all other factors (including the oxide used for the electrode), there is still a net gain in efficiency.

Another efficiency parameter which is obtainable from the data set is the “power efficiency” parameter. This is the ratio of cell power density (mW/cm^2) to the total

irradiance, calculated from the 1 sun J/V plot (which uses a standard 100mW/cm^2 irradiance).

$$\eta_{power} = \frac{P_{max}/A_{cell}}{100mW\,cm^{-2}}$$

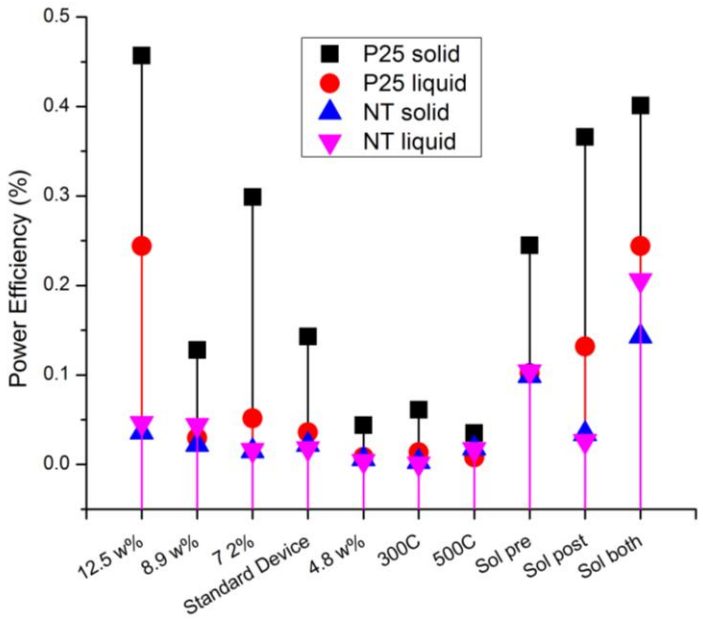

Figure 17: Power efficiency plot in percent, sorted by process parameter.

Comparing the power efficiency across all parameters, it can again be seen that the anatase electrode devices with solid electrolyte perform best overall, with sol gel treatment further improving the performance of those. Higher deposition concentration improves the anatase devices significantly as well. The nanotube devices are overall able to use a smaller fraction of the power hitting their active surface, but their function is improved to some extent by higher deposition concentration and processing temperature. The use of a blocking layer (sol pretreatment) is a significant improving factor for nanotube cells, especially as compared to the level of improvement seen in other device types, and the very

best nanotube cells do outperform the worst anatase cells. This is not helped by the addition of the solid electrolyte, however, which produces no improvement in the nanotube cells, and in most cases results in worsened performance.

Dye Loading Investigation

The ability of a metal oxide electrode to be loaded with a large quantity of dye is largely dependent on its surface area. Loading dye from a solution at known concentration on a film of known mass, then determining the concentration of remaining dye allows determination of the degree to which the electrode surface area is available as an anchor point for dye molecules This differs from a direct measurement of surface area by gas adsorption primarily by failing to show any effect from surface area unavailable to the dye (for instance, in very small pores). Measurements were made at 18 and at 65 hours of immersion, which allowed for some assessment of the speed of the dye-loading process.

In advance, a 0.3mM solution of N719 in absolute ethanol was prepared. This solution was then assessed with UV-Visible absorption spectroscopy to assess concentration with higher precision, in reference to the published value of the extinction coefficient of the dye in solution ($13{,}500\ M^{-1}g^{-1}$ at 530nm)[23]. Nanotube and anatase films of known mass were prepared by doctor blading (5.74 wt% oxide, 400C

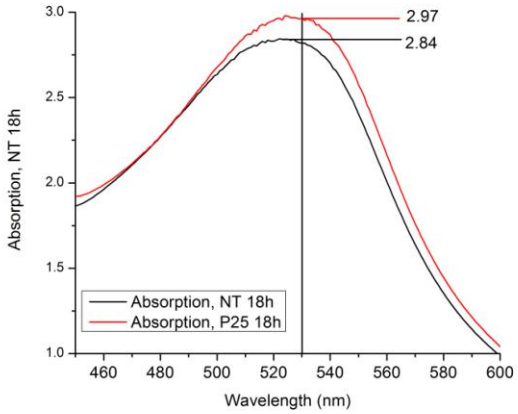

Figure 18: 530nm absorption peak for ethanolic N719 solution removed from nanotube and anatase films at 18h.

sinter, no chemical treatment) and weighing when they had cooled after heat treatment. The samples were each sealed in an airtight vial with 1.500g N719 solution, and left for 18 hours, at which point 1mL of solution was removed and measured under UV-Vis absorption (figure 42). Concentration was determined from the Beer-Lambert law: $A = l * c * \epsilon(\lambda)$, and where path length (l) is defined by use of a 1cm UV-Vis cuvette.

From these measurements, the concentrations were determined to be: 2.10×10^{-4} M for the nanotube film and 2.20×10^{-4} M for the anatase film at 18 hours, corresponding to a dye loading of 3.10×10^{-7} mol/g for the nanotube film, and 5.22×10^{-7} mol/g for the anatase film.

References:

23. M. Zukalova et al, *Nano Lett.*, **5,** (2005)

IV: Conclusions

The experimental results discussed in this report pertain to the comparative performance of titania electrodes for dye-sensitized solar cells, prepared from different starting materials, and treated under a varied set of conditions. In the broadest sense, it is clear from the prior discussion that titanate nanotubes do not compare favorably to anatase titanium dioxide for a solution-deposited electrode material in the dye-sensitized solar cell. Electrodes made from the nanotube material showed poorer performance than those from the anatase material in almost all cell preparations, and achieving only parity in the best case (isopropoxide pre- and posttreatment, liquid electrolyte), for which Raman spectroscopic results indicate total crystal conversion to the anatase phase.

The difference in performance between electrode materials is amplified by the substitution of solid plasticized electrolyte for liquid. Electrodes deposited from the anatase slurry demonstrated an improvement in device parameters, showing higher power output, V_{oc}, J_{sc}, better resistance to leakage current, and improved fill factor. Nanotube devices also showed improvement of shunt resistance and fill factor, but performed uniformly worse in terms of current and power generation, making them less effective solar cells overall. This trend also persisted, regardless of the variations employed in device preparation.

The key to this difference in performance is highlighted by the results of the set of SEM measurements, showing significant voids between individual ~10μm aggregates of densely packed, quasi-one dimensional crystallites which form highly continuous surfaces

at the nanometer scale, except for the minority regions of randomly oriented tubelike material with ~10nm pores. This is strikingly different from the structure of the anatase films, which are monolithic at the scale of tens of microns and are massively porous at the scale of tens of nanometers. The low current density of the nanotube films is likely due to the micron-scale structure, with relatively low connectivity between individual aggregates (especially as compared to the anatase films). The lack of nanometer pores can be expected to further reduce the current in two key ways: first, the lack of surface area leads to reduced dye loading as shown by UV-Vis of the dye solution, and second, the lack of porosity results in poor infiltration by the electrolyte (exacerbated with the large-molecule solid electrolyte) limiting dye regeneration and consequently reducing photocurrent.

The comparative changes in performance on switching from liquid electrolyte to solid electrolyte seem indicative of further interesting properties of the anatase system compared with the nanotube system. In particular, the improved performance of one, compared with the reduced performance of the other indicates an effect depending on porosity. As discussed in the introduction, parasitic recombination can be limited by reducing the degree of contact between the redox medium and uncoated regions of the titania, such as pores too small to be infiltrated during dye-loading. An advantage in this respect of the solid electrolyte is that the large size of the PEO molecule (4M molecular weight) should limit the infiltration of the electrolyte into regions inaccessible to the dye, minimizing contact between oxidized triiodide ions and reductive electrons in the titania. The scanning electron micrographs of polymer-oxide blends indicate, however, that the infiltration of polymer into the anatase films is not limited to an extent that prevents significant contact between the phases. By comparison, the films made from nanotubes

show limited infiltration (as evidenced by presence of polymer at cracks in the film), indicating that the significantly lower porosity of those films tends to produce greater phase separation and lower infiltration.

The overall indication of these results is that due to aggregation during solvent evaporation and reduction of porosity during the thermal treatment necessary to promote connectivity, titanate nanotubes work poorly for simple solution deposition as a solar cell electrode. This study also demonstrates a simply-deposited anatase electrode which experiences an improvement of performance when used with a polymeric electrolyte as compared to a liquid solution in acetonitrile, again apparently due to the nature of the pores formed during solvent evaporation and thermal treatment. The solid electrolyte devices produced in this study show power production and current density comparable to other published results, without a complex deposition procedure or the use of film additives to control aggregation.

The application of this technique, however, is ultimately of limited interest. In contemporary cells of noteworthy quality, a dedicated chemical treatment (4-*tert*-butylpyridine) is applied to reduce the rate of back-reaction, which appears to be the same function performed by the use of solid electrolyte. Cells produced with state-of-the-art liquid electrolyte, more sophisticated oxide deposition, and a dedicated recombination blocking layer have higher fill factor and efficiencies which (as noted earlier) approach 10% power conversion.